J Comput Aided Mol Des
DOI 10.1007/s10822-017-0045-2

Biologically relevant conformational features of linear and cyclic proteolipid protein (PLP) peptide analogues obtained by high-resolution nuclear magnetic resonance and molecular dynamics

Golfo G. Kordopati[1] · Haralambos Tzoupis[1] · Anastassios N. Troganis[2] · Gerasimos M. Tsivgoulis[1] · Simona Golic Grdadolnik[3] · Carmen Simal[1] · Theodore V. Tselios[1]

Received: 21 May 2017 / Accepted: 26 July 2017

Abstract Proteolipid protein (PLP) is one of the main proteins of myelin sheath that are destroyed during the progress of multiple sclerosis (MS). The immunodominant $PLP_{139–151}$ epitope is known to induce experimental autoimmune encephalomyelitis (EAE, animal model of MS), wherein residues 144 and 147 are recognized by T cell receptor (TCR) during the formation of trimolecular complex with peptide-antigen and major histocompability complex. The conformational behavior of linear and cyclic peptide analogues of PLP, namely $PLP_{139–151}$ and cyclic (139–151) (L^{144}, R^{147}) $PLP_{139–151,}$ have been studied in solution by means of nuclear magnetic resonance (NMR) methods in combination with unrestrained molecular dynamics simulations. The results indicate that the side chains of mutated amino acids in the cyclic analogue have different spatial orientation compared with the corresponding side chains of the linear analogue, which can lead to reduced affinity to TCR. NMR experiments combined with theoretical calculations pave the way for the design and synthesis of potent restricted peptides of immunodominant $PLP_{139–151}$ epitope as well as non peptide mimetics that rises as an ultimate goal.

Keywords Proteolipid protein · Cyclic peptide · Nuclear magnetic resonance · Molecular dynamics · Conformational analysis

Introduction

Multiple sclerosis (MS) is a chronic inflammatory and demyelinating disease of the central nervous system (CNS) that causes progressive degeneration of nerve cell axons [1, 2]. The disease is triggered by the formation of the trimolecular complex between the T cell receptor (TCR), the corresponding antigenic epitopes of myelin proteins and major histocompatibility complex (MHC) or human leukocyte antigen (HLA) receptor, with the subsequent stimulation of encephalitogenic T cells [3]. Myelin basic protein (MBP), proteolipid protein (PLP), myelin oligodendrocyte glycoprotein (MOG) and myelin-associated glycoprotein (MAG) in the CNS are the main myelin proteins surrounding nerve cells [4]. While all of these proteins have been shown to be potential auto-antigens that can lead to induction of autoimmunity [4], PLP and MBP have been widely studied since they constitute the two major proteins of the myelin sheath [5]. In this light, PLP has emerged as myelin-related target antigen with a clearly-defined encephalitogenic T cell response in animal models of MS [6–10].

The encephalitogenic epitopes derived from PLP in SJL/J mice, are the $PLP_{40–70}$, $PLP_{100–119}$, $PLP_{139–151}$ and $PLP_{178–191}$ [11–13]. $PLP_{139–151}$, with the sequence H^{139}CLGKWLGHPDKF^{151} or with serine substitution at position 140, instigates the most profound immune responses in SJL/J mice [13]. Previous studies indicate that residues Trp^{144} and His^{147} of $PLP_{139–151}$ are crucial for interactions with TCR [10, 14], while other residues, such as Leu^{141}, are reported as secondary TCR contact sites

Electronic supplementary material The online version of this article (doi:10.1007/s10822-017-0045-2) contains supplementary material, which is available to authorized users.

✉ Theodore V. Tselios
ttselios@upatras.gr

[1] Department of Chemistry, University of Patras, 26504 Patras, Greece

[2] Department of Biological Applications and Technology, University of Ioannina, 45110 Ioannina, Greece

[3] Department of Biomolecular Structure, National Institute of Chemistry, 1001 Ljubljana, Slovenia

Published online: 29 July 2017

[14]. Nevertheless, the amino acids that have been shown to interact strongly with the MHC receptor are mainly Leu^{145} and Pro^{148} [14]. Based on these precedents, altered peptide ligands (APLs) of $PLP_{139–151}$, with substitutions in positions 144 and 147, with Leu and Arg respectively, have been addressed; resulting in decreased binding affinity to TCR and EAE induction in mice [14]. A number of rationally designed linear and cyclic peptide analogues of immunodominant epitopes of myelin proteins have been prepared and studied by our research group [15, 16]. Notably, the synthetic cyclic peptides, with severely reduced conformational flexibility, have proved to increase the in vivo stability [17–19]; as a result of their increased bioavailability, resistance to proteolytic degradation and improved receptor selectivity. Hence, cyclic peptides compared to their linear counterparts can be considered as preferred candidates for the rational design of therapeutic molecules. However, since cyclic peptides are more conformationally restrained, theoretical studies or experimental evidence are necessary to ensure the retention of the bioactive conformation [15, 17, 20].

The characterization of the synthetic analogues was performed in aqueous solution using high field 2D nuclear magnetic resonance (NMR) to examine bioactive conformers of biologically important molecules [21, 22]. Along with molecular modeling techniques, 2D NMR is a useful tool for structure-based drug design. The information derived from the combination of these two techniques (conformation and stereochemical properties), can offer valuable insight in the study of biological molecules in an environment, which resembles the conditions in the living cells. We have implemented the particular combination of techniques, along with biological experiments, in order to assess the potency of synthesized antagonists in MS induction [23–26]. Herein, we report the conformational analysis, using 2D NMR and molecular dynamic (MD) simulations, of serine 140 substituted linear $PLP_{139–151}$ and cyclic (139–151) (L^{144}, R^{147}) $PLP_{139–151}$ ($H^{139}SLGKL^{144}LGR^{147}PDKF^{151}$) peptide analogues, in water solution.

Materials and methods

Synthesis of $PLP_{139–151}$ and cyclic (139–151) (L^{144}, R^{147}) $PLP_{139–151}$ peptides

The synthesis of $PLP_{139–151}$ ($H^{139}SLGKWLGHPDKF^{151}$) and cyclic (139–151) ($L^{144}$, R^{147}) $PLP_{139–151}$ ($H^{139}SLGKL^{144}LGR^{147}PDKF^{151}$) was accomplished using the Fmoc/tBu methodology and 2-chlorotrityl chloride (CLTR-Cl) resin (Supporting information Table S1 and Scheme S1) [27–30]. The first N^{α}−Fmoc-protected amino acid (Fmoc-Phe-OH) was esterified to the resin, in the presence of *N,N*-diisopropylethylamine (DIPEA) in dichloromethane (DCM). The rest of the peptide chain was assembled by sequential couplings of the corresponding protected amino acids, in the presence of *N,N′*-diisopropylcarbodiimide (DIC) and 1-hydroxybenzotriazole (HOBt) in *N,N*-dimethylformamide (DMF). Head-to-tail cyclization of the protected peptide was performed by a drop-wise addition of a solution of the desired linear protected peptide, 2,4,6-collidine and 1-hydroxy-7-azabenzotriazole (HOAt) in dry DMF to a solution of O-(benzotriazol-1-yl)-*N,N,N′,N′*-tetramethyluroniumtetrafluoroborate (TBTU) in DMF for 4 h [17, 19, 31]. Final side chain deprotection of protected peptides was achieved using trifluoroacetic acid (TFA) in DCM, in the presence of triethylsilane (TES) and dithiothreitol (DTT) as scavengers. Purification of crude peptides was performed on a semi-preparative high performance liquid chromatography (HPLC) using LiChrosorb RP-18 column. Peptide purity was determined by analytical RP-HPLC using an Agilent ZORBAX Eclipse Plus C18 column (3.5 μm, 100×4.6 mm) whereas identification was achieved by electron spray mass spectrometry (ESI-MS) and NMR.

NMR spectroscopy

The NMR spectra were recorded on a Bruker AVANCE 500 MHz and a Varian DirectDrive 800 MHz spectrometers at 298 K. Ultra-precision 5 mm NMR tubes from Norell were used, containing 1 mM of the peptide analogue in 0.7 mL H_2O:D_2O (9:1) as solvent. D_2O was purchased from Alfa Aesar, Karlsruhe Germany. At this concentration, no line broadening effects, which indicate aggregation of peptides, were observed.

2D NMR spectra of linear $PLP_{139–151}$ were recorded on a Bruker AVANCE 500 MHz spectrometer at 298 K. They were acquired using the TPPI method for quadrature detection. The 2D spectra were recorded using 512 increments of 2 K complex data points and 80 scans per increment for ROESY and 16 scans for TOCSY experiment, respectively. The mixing time for the ROESY spectra was 200 ms while that for TOCSY was 80 ms. The WATERGATE-5 pulse sequence was used for water suppression. Data were processed using the TopSpin standard software. The t_1 dimension was zero-filled to 1 K real data points, and 60 phase-shifted square sine bell window functions were applied in both dimensions.

2D spectra of cyclic (139–151) (L^{144}, R^{147}) $PLP_{139–151}$ were recorded on a Varian DirectDrive 800 MHz spectrometer at 298 K. They were collected in the phase sensitive mode, using pulse sequences and phase-cycling routines provided in Varian libraries of pulse programs. The cryogenic triple-resonance NMR probe

Table 1 ^{1}H chemical shift assignments of linear $PLP_{139–151}$ in H_2O:D_2O (9:1), at 298 K and 500 MHz

Amino acids	NH	α	β	γ	δ	Other protons
His^{139}	–	4.20	3.22	–	–	2H:8.47 4H:7.23
Ser^{140}	8.74	4.38	3.72	–	–	–
Leu^{141}	8.53	4.28	1.53	1.48	0.78	–
Gly^{142}	8.10	3.70 3.74	–	–	–	–
Lys^{143}	8.05	4.10	1.48	1.10	δCH:1.44	εCH:2.75 NH:7.37
Trp^{144}	8.17	4.57	3.04 3.12	–	–	4H:7.46, 7H:7.28, 6H:7.03, 5H:6.95, 2H:7.07, NH:10.02
Leu^{145}	7.91	4.07	1.49	1.32	0.63 0.71	–
Gly^{146}	7.39	3.41 3.54	–	–	–	–
His^{147}	7.99	4.76	2.89 3.02	–	–	2H:8.40 4H:7.06
Pro^{148}	–	4.24	2.10	1.81 1.73	3.54 3.41	–
Asp^{149}	8.44	4.47	2.62	–		–
Lys^{150}	8.01	4.07	1.54	1.12	δCH 1.46	εCH 2.75 NH:7.37
Phe^{151}	7.95	4.43	2.83 3.05	–	–	2,6H:7.09 3,5H:7.17 4H:7.12

was used. The spectra were acquired with a spectral width of 8803 Hz, 4096 data points in t_2, 16–64 scans, 512 complex points in t_1, and a relaxation delay of 1.5 s. In the DQF-COSY experiment gradients were used for the coherence selection and the WATERGATE pulse block for the water suppression. The mixing times in the NOESY and TOCSY were 150 and 60 ms, respectively. The residual water signal in TOCSY and NOESY was suppressed using excitation sculpting and adiabatic pulses were applied for suppression of zero quantum

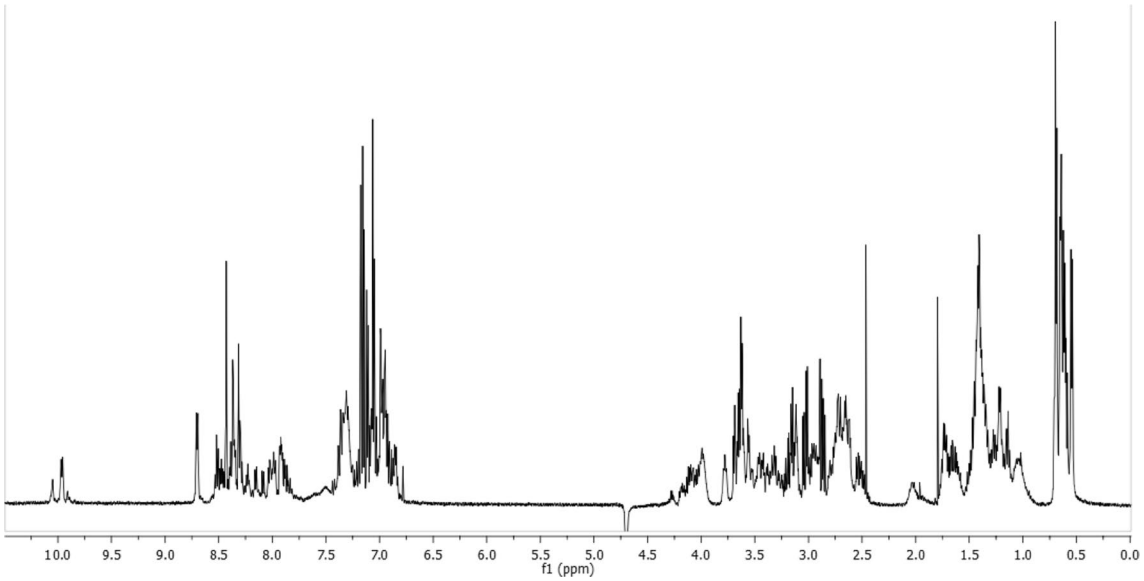

Fig. 1 ^{1}H NMR spectrum of $PLP_{139–151}$ in H_2O:D_2O (9:1) recorded at 500 MHz and 298 K

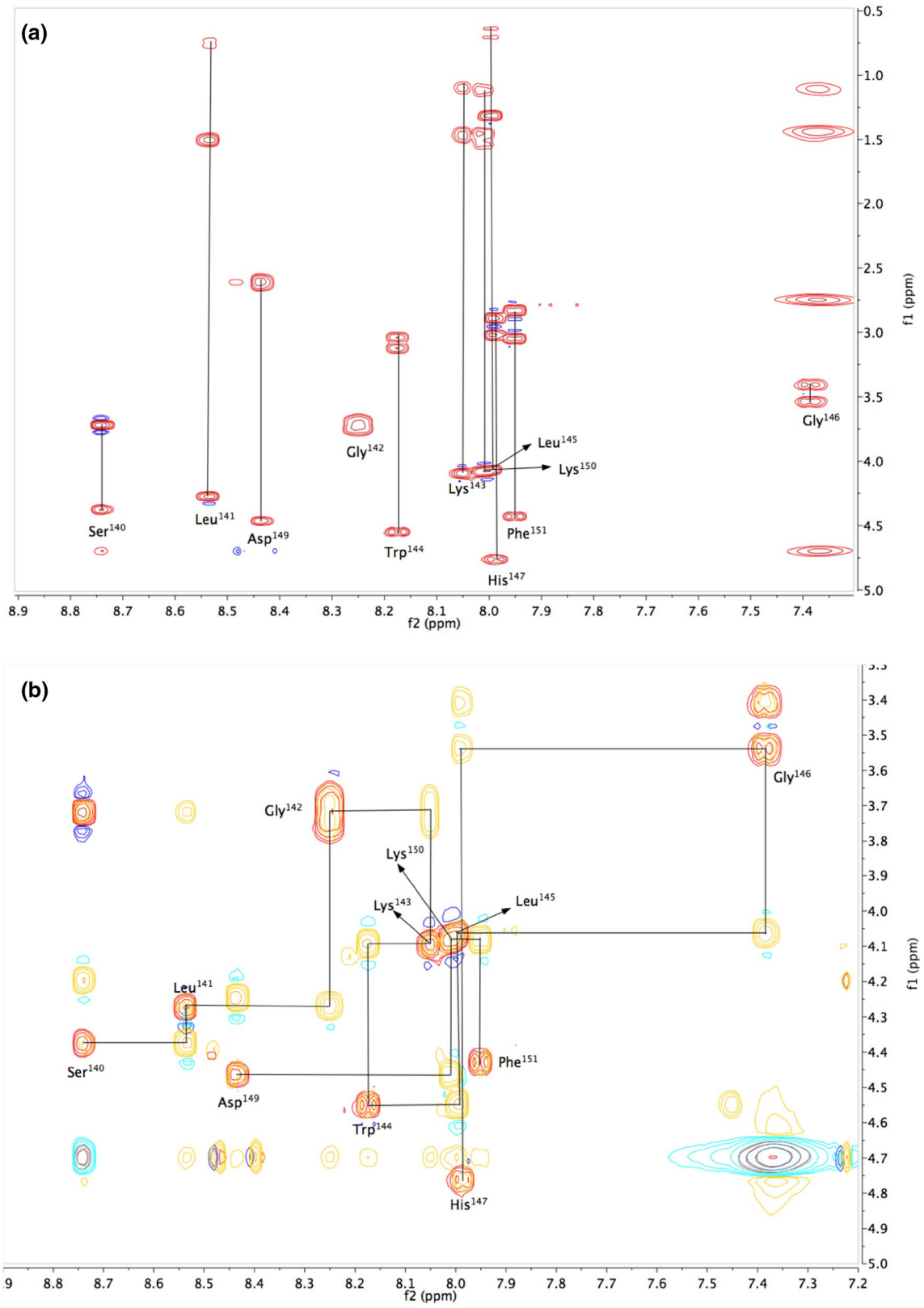

Fig. 2 2D TOCSY/ROESY spectra of $PLP_{139–151}$ obtained at 500 MHz and 298 K; **a** expanded region of the TOCSY spectrum; **b** expanded region of the superimposed TOCSY/ROESY spectra for the peptide backbone

Table 2 Intensities of the observed inter-residue cross-peaks in the ROESY spectrum for linear $PLP_{139–151}$

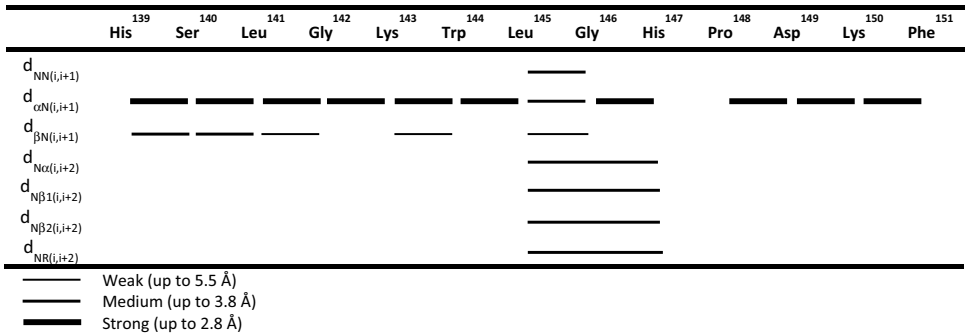

The results were obtained at mixing time of 200 ms in H_2O:D_2O (9:1), at 298 K and 500 MHz

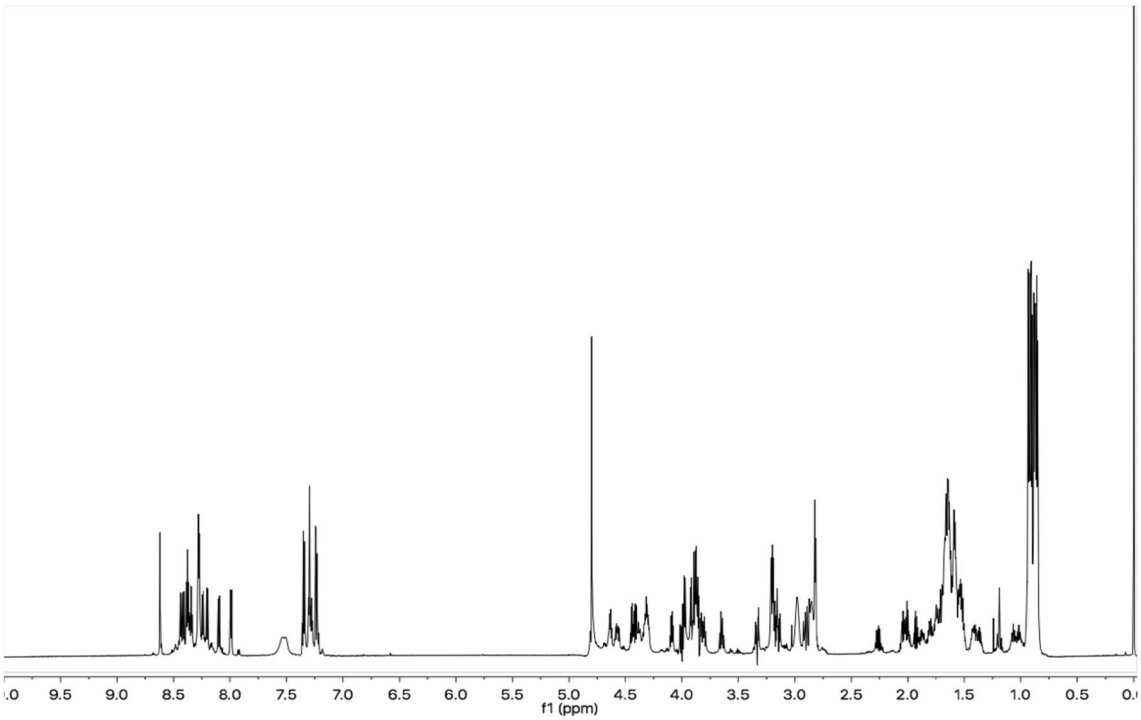

Fig. 3 ^{1}H NMR spectrum of cyclic (139–151) (L^{144}, R^{147}) $PLP_{139–151}$ in H_2O:D_2O (9:1) recorded at 800 MHz and 298 K

artifacts during mixing time. Spectra were processed and analyzed with the FELIX 2007 software package from Felix NMR Inc.

Unrestrained MD simulations

The construction of $PLP_{139–151}$ (H^{139}SLGK**W**LG**H**PDKF^{151}) and cyclic (139–151) (L^{144}, R^{147}) $PLP_{139–151}$ (H^{139}SLGK**L**^{144}LG**R**^{147}PDKF^{151}), was performed using the USCF Chimera software [32]. The amino acids, comprising the peptide, were placed in sequence with no initial secondary structure assignment (unfolded conformation). The systems were subjected to all-atom unrestrained MD simulations in explicit solvent using the AMBER14 software [33].

MD simulation of linear/cyclic PLP analogues in water

The AMBER force field ff14SB [34] has been implemented for the construction of $PLP_{139–151}$ peptide parameters. The tleap module of AMBER14 was utilized for the topology and coordinate files used in the MD simulations. The solvation of the system was performed using the TIP3P water model [35]. The peptide was enclosed in a truncated octahedral box (cutoff distance of 10 Å) and periodic boundary conditions were applied to the system. The next step involved the minimization of the peptide, followed by heating from 0 to 300 K for 100 ps (under constant volume) using the Langevin dynamics temperature scaling [36]. Constant pressure equilibration was also accomplished, for another 100 ps. Both heating and pressure equilibration were achieved by imposing a 10 kcal/(mol × Å^2) restraint

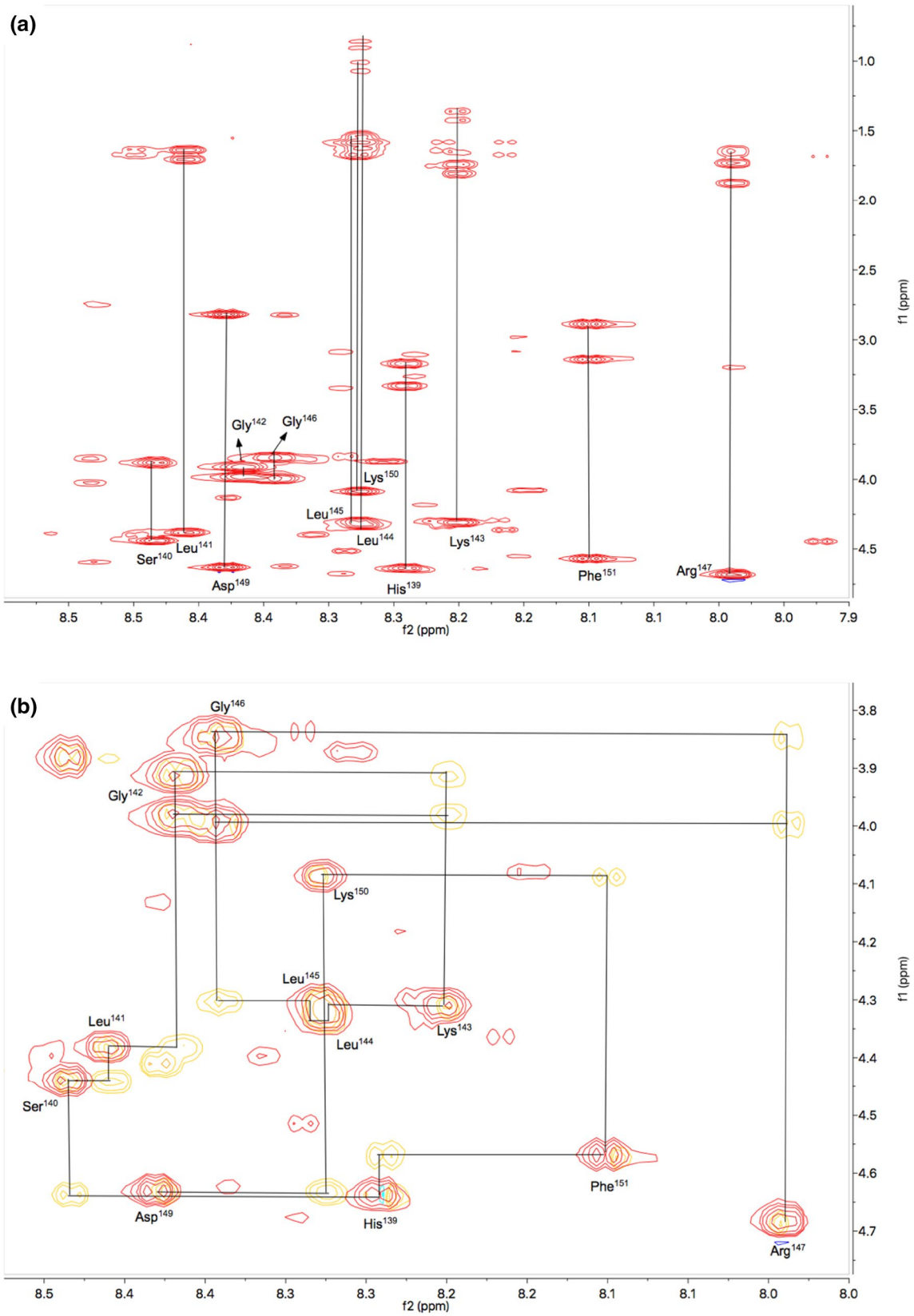

Fig. 4 2D TOCSY/NOESY spectra of cyclic (139–151) (L^{144}, R^{147}) $PLP_{139–151}$ obtained at 800 MHz and 298 K; **a** expanded region of the TOCSY spectrum; **b** expanded region of the superimposed TOCSY/NOESY spectra for the peptide backbone

Table 3 Intensities of the observed inter-residue cross-peaks as recorded in the NOESY spectrum of cyclic (139–151) (L^{144}, R^{147}) $PLP_{139–151}$

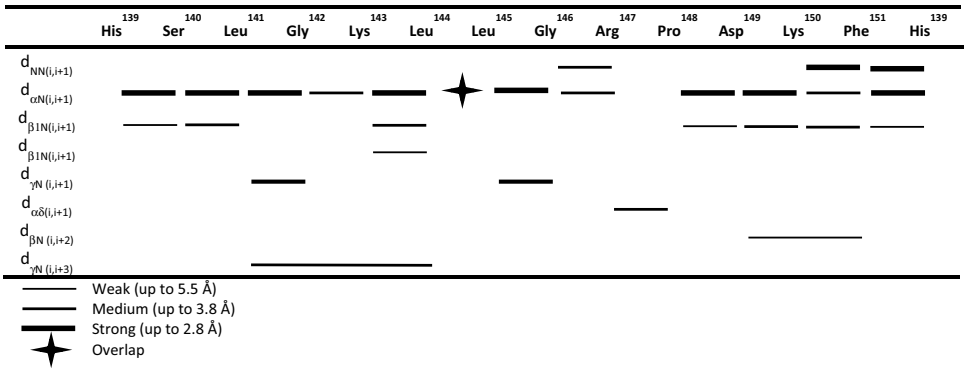

The results were obtained at mixing time of 150 ms in H_2O:D_2O (9:1), at 298 K and 800 MHz

on the solute. The equilibration step was prolonged for a further 200 ps, after removing all restraints. Six individual MD production runs were performed for 100 ns each (total of 600 ns) in the NPT ensemble (isothermal and isobaric conditions) for $PLP_{139–151}$ and one MD production run for 100 ns for cyclic (139–151) (L^{144}, R^{147}) $PLP_{139–151}$ form. The Langevin thermostat, with a collision frequency of 2 ps^{-1}, was used to keep the temperature constant. The bonds involving hydrogen atoms were kept to their equilibrium distance with the SHAKE algorithm [37]. The long range electrostatic interactions were calculated using the Particle Mesh Ewald (PME) method [38].

Trajectory and clustering analysis

The analyses (RMSD, atomic fluctuations, and clustering calculations) performed on all the AMBER MD trajectories were carried out using the cpptraj module [39] of the AMBER14 molecular package. The analysis of hydrogen bond (HB) interactions was based on geometric criteria. The limitations imposed were a 3.5 Å cutoff for donor–acceptor distance and a donor-hydrogen-acceptor angle cutoff of 120°. The hierarchical method [40] was applied for the grouping process in the various MD trajectories, with the RMSD imposed as the distance metric (cutoff 2.5 Å).

Results and discussion

NMR conformational analysis

Conformational analysis of linear $PLP_{139–151}$

The structure elucidation of $PLP_{139–151}$ was achieved using a combination of ^{1}H NMR, TOCSY and ROESY experiments. The proton chemical shifts, recorded in the ^{1}H NMR, along with the assignment of the peaks are reported in Table 1. The ^{1}H NMR spectrum of the linear peptide presents one set of clearly resolved signals (Fig. 1) in aqueous solution. The identification of amino acid spin patterns was achieved through the analysis of the scalar and spatial connectivities as provided by the TOCSY and ROESY experiments, respectively (Fig. 2). The spin system of Ser^{140} at 8.75 ppm in TOCSY spectrum (Fig. 2a) was employed as a reference point for the peak assignment. As depicted in Fig. 2b, the combination of TOCSY and ROESY experiments based on the ROE signals between $H^{\alpha}_{(i)}$ and $H^{N}_{(i+1)}$ allows the establishment of backbone sequential connectivities for the entire peptide and resolves the specific assignments for all the resonances (Figs. 1, 2; Table 1).

Based on the integrations of the ROESY cross-peaks, the information for the spatial vicinity of protons in the molecule is provided (Table 2). The strong ROE connectivities between $H^{\alpha}_{(i)}$ and $H^{N}_{(i+1)}$ along the entire backbone of $PLP_{139–151}$ indicate an extended backbone conformation for the peptide (Table 2 and Table S2). Only in the region between the residues 145–147 another secondary structure element is observed. Four cross-peaks between $H^{N}_{(i)}$–$H^{\alpha}_{(i+2)}$, $H^{N}_{(i)}$-$H^{\beta1}_{(i+2)}$, $H^{N}_{(i)}$–$H^{\beta2}_{(i+2)}$ and $H^{N}_{(i)}$–$H^{R}_{(i+2)}$, of medium or weak strength are recorded in this peptide region indicating the presence of folded conformation between Leu^{145} and His^{147} residues. The deviation from the extended conformation in this region of $PLP_{139–151}$ is further supported by the presence of a $H^{N}_{(i)}$–$H^{N}_{(i+1)}$ cross peak between Leu^{145} and Gly^{146}.

Conformational analysis of cyclic (139–151) (L^{144}, R^{147}) $PLP_{139–151}$

The peak assignment for the cyclic PLP analogue was performed following the same protocol described for the linear peptide (Table S3). As with the linear $PLP_{139–151}$, the spectrum for the cyclic form of the peptide presents one set of clearly resolved signals (Figs. 3, 4). The combination of TOCSY and NOESY spectra (Fig. 4) were utilized to

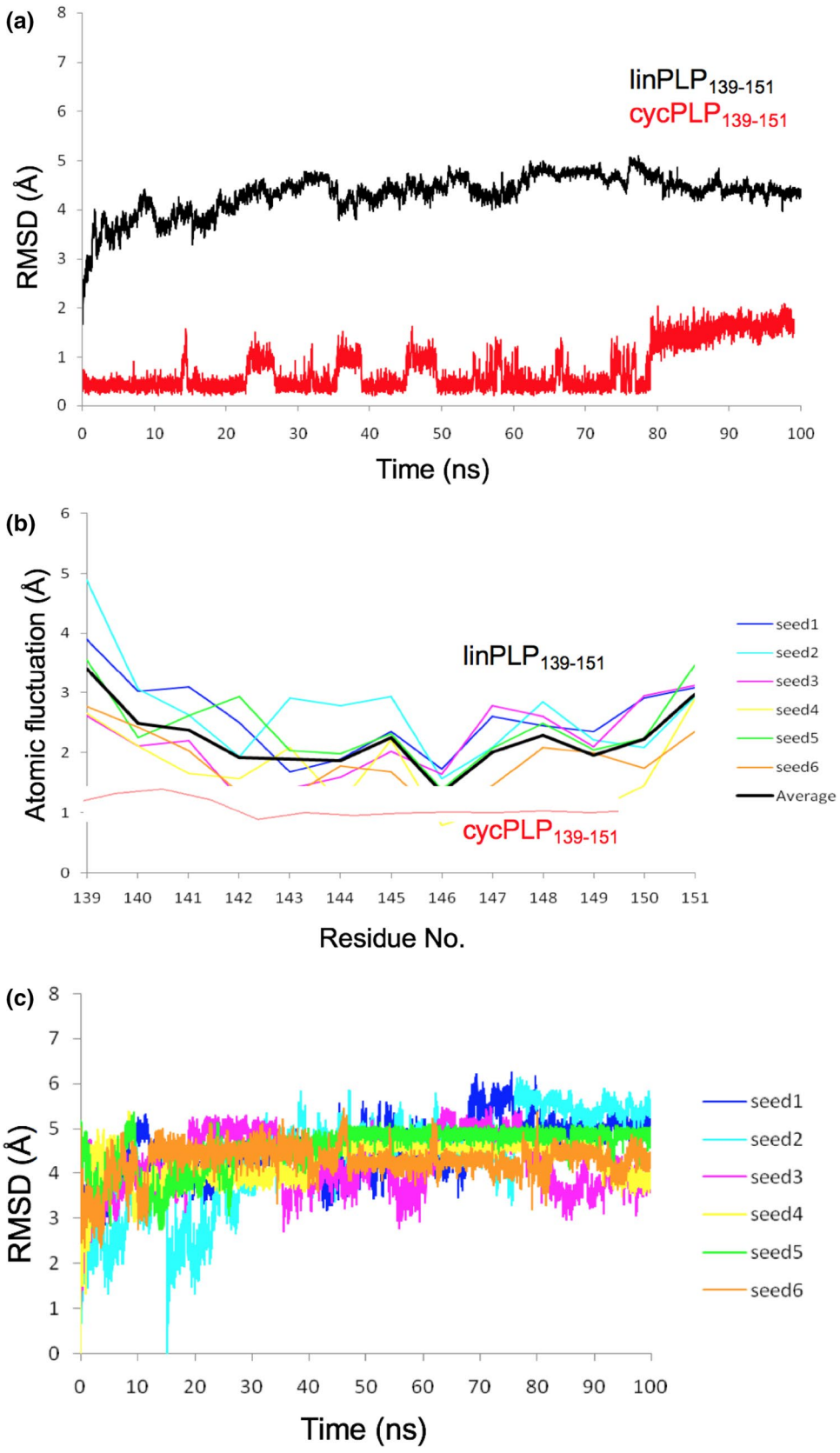

Fig. 5 **a** RMSD for the backbone C^{α} atoms in comparison to a common starting conformation: in *black* the average RMS value of all the MD production runs for $PLP_{139–151}$ and in *red* the RMS values over time for the cyclic peptide; **b** atomic positional fluctuations of the residues for both the linear and cyclic peptide analogues; **c** RMS values over time for the different MD production runs of $PLP_{139–151}$

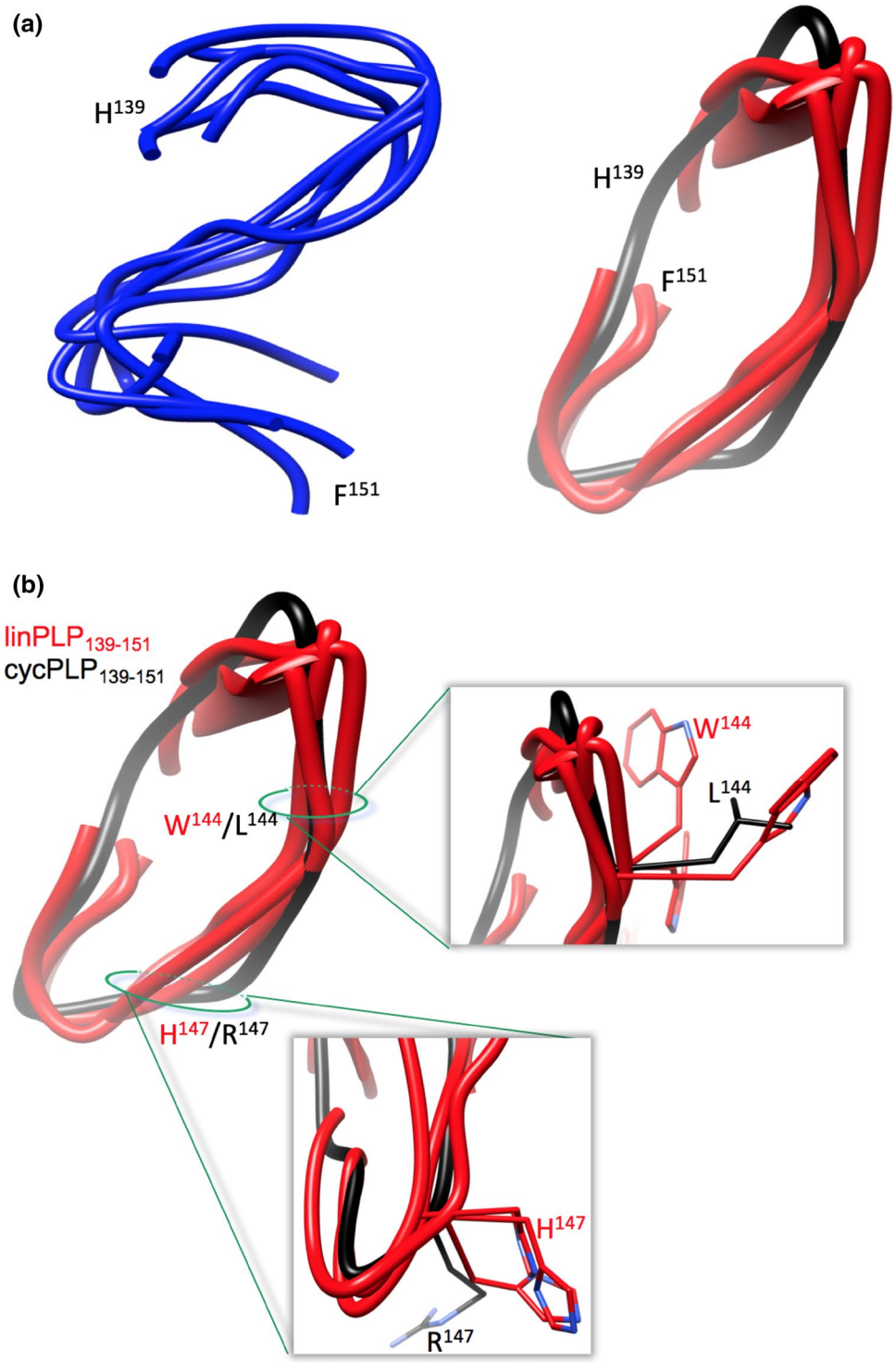

Fig. 6 **a** Representative conformations of $PLP_{139–151}$ (*blue* and *red*) and cyclic (139–151) (L^{144}, R^{147}) $PLP_{139–151}$ (*black*) peptides based on the clustering analysis performed on the different MD simulations; **b** comparison of the mutation site residues between the cyclic forms of $PLP_{139–151}$ (*red*) and cyclic (139–151) (L^{144}, R^{147}) $PLP_{139–151}$ (*black*) analogue. The enclosed figures depict the differentiation at positions 144 and 147

identify the spin patterns of the cyclic PLP analogue. The spin system of Ser^{140} at 8.45 ppm (Fig. 4a) was employed as a reference point.

The amide bond between residues His^{139} and Phe^{151}, that is the result of the cyclization process, is indicated in the NOESY spectrum through the presence of two NOE signals between protons $H^{\alpha}_{(i)}$ and $H^{N}_{(i+1)}$ and $H^{N}_{(i)}$–$H^{N}_{(i+1)}$ (Fig. 4b). The analysis of the spectra and the subsequent peak assignment showed different pattern of NOEs (Table 3) as for the linear analogue (Table 2). This result indicates a different backbone conformational propensities of residues between the two analogues.

Unrestrained molecular dynamics

Molecular dynamics simulation of linear/cyclic PLP analogues

The small length of the peptide, only 13 residues, allows greater mobility in the MD simulation of $PLP_{139–151}$ (Fig. 5a, black). The RMSD values recorded over the simulation time reflect the changes observed in its conformations. On the other hand, the cyclic analogue presents a more stable conformation over time (Fig. 5a, red). The highest RMSD value during the simulation of the cyclic peptide is 1.9 Å (Fig. 5a, red). The low RMSD for cyclic (139–151) (L^{144}, R^{147}) $PLP_{139–151}$ is an expected observation (Fig. 5a, red) since the cyclization of the peptide should restrict the movement of the backbone atoms. Hence, the only mobility arises from the restricted movement of the amino acids' side chains. The expected differences between the two PLP peptide analogues (linear and cyclic) are also mirrored in the atomic fluctuations of the residues (Fig. 5b). The residues in $PLP_{139–151}$ show increased mobility (Fig. 5b, black) than the respective residues in cyclic (139–151) (L^{144}, R^{147}) $PLP_{139–151}$ analogue (Fig. 5b, red). Furthermore, the RMSD values of the linear peptide follow a similar pattern, which is indicative of a similar behaviour for the peptide in the independent MD production runs (Fig. 5c).

The clustering analysis performed on the MD simulation of $PLP_{139–151}$ reveals that the different conformations of the peptide are clustered in two main groups (Fig. 6a, blue and red). The representative conformations of the linear peptide in water show the adoption of a "sigmoidal" form (Fig. 6a, blue). That configuration is dominant for the majority of time in all the different MD simulations (Table 4), while the "cyclic" conformation (Fig. 6a, red) is present in a smaller fraction of time at various seeds (Table 4). The rest of the conformations adopted by $PLP_{139–151}$, are a mixture of interchangeable forms between the "sigmoidal" and "cyclic" structures. As mentioned previously, in cyclic (139–151) (L^{144}, R^{147}) $PLP_{139–151}$ analogue the extensive changes in the conformations of the peptide throughout the MD simulation are not allowed (Fig. 5a, red). The restricted conformational changes in the cyclic peptide, reported here, are in agreement with previous observations in synthesized cyclic analogues of different epitopes of myelin proteins [15, 17, 41].

The "cyclic" conformation of the linear analogue in aqueous solutions closely resembles that of cyclic (139–151) (L^{144}, R^{147}) $PLP_{139–151}$ analogue (Fig. 6a, red and black). The differences between the "cyclic" forms (Fig. 6a, red), adopted by the linear peptide during the simulation time, and the cyclic analogue (Fig. 6a, black) are centred on the mutation sites. The substitution of His^{147} (in linear $PLP_{139–151}$) with Arg^{147} [in cyclic (139–151) (L^{144}, R^{147}) $PLP_{139–151}$] changes the orientation of the Arg side chain (guanidino group) in the cyclic peptide and is positioned away in comparison to the linear analogue (Fig. 6b, red and black). In both cases, though, the residue neighbouring Pro^{148} retains its orientation towards the solvent. Moreover, there is no retention of configuration in position 144 between the cyclic conformations adopted by the linear analogue and cyclic (139–151) (L^{144}, R^{147}) $PLP_{139–151}$ (Fig. 6b, red and black). The calculation of the potential energy (E_{Ptot}) for the representative conformations of $PLP_{139–151}$, shows that both the sigmoidal and cyclic forms preferred, present comparable values (Table 4; Fig. 7). The cyclic conformations adopted by the linear analogue have a higher E_{Ptot} than the respective sigmoidal forms (Table 4). This could be attributed to the restrictions imposed in the movement of the backbone atoms by the cyclic form. On the other hand, the lowest potential energy is observed for the dominant representation ("sigmoidal") adopted by the linear peptide with a value of $-1.901/-2.966 \times 10^4$ kcal/mol (Table 4; Fig. 7). An important feature highlighted by the comparison of the cyclic analogue and the dominant conformation with the lowest potential energy is the orientation of the amino acids side chains (Fig. 7, blue and black). Similarly to the "cyclic" forms adopted by the linear peptide, the side chain of His^{147} in "sigmoidal" form, is oriented away from the position obtained from Arg^{147} in

Table 4 Summary of the clustering analysis for the diverse MD simulations of linear $PLP_{139–151}$ and the potential energy of the different representative conformations

MD simulations	Presence (%)[a]	Single point[b]	Optimised[b]
Seed 1			
Cluster 1	62	−1.630	−2.584
Seed 2			
Cluster 1[c]	26	−1.222	−2.199
Cluster 2	41	−1.398	−2.275
Seed 3			
Cluster 1	47	−1.478	−2.340
Cluster 2[c]	21	−1.277	−2.254
Seed 4			
Cluster 1	53	−1.901	−2.966
Cluster 2[c]	23	−1.446	−2.369
Seed 5			
Cluster 1	46	−1.452	−2.366
Seed 6			
Cluster 1	39	−1.240	−2.034

[a]Presence of the particular conformation as a percentage of simulation time in each MD simulation run

[b]Values of the potential energy in ($\times 10^4$) kcal/mol

[c]The cyclic conformations adopted by the linear analogue in the different MD simulation runs

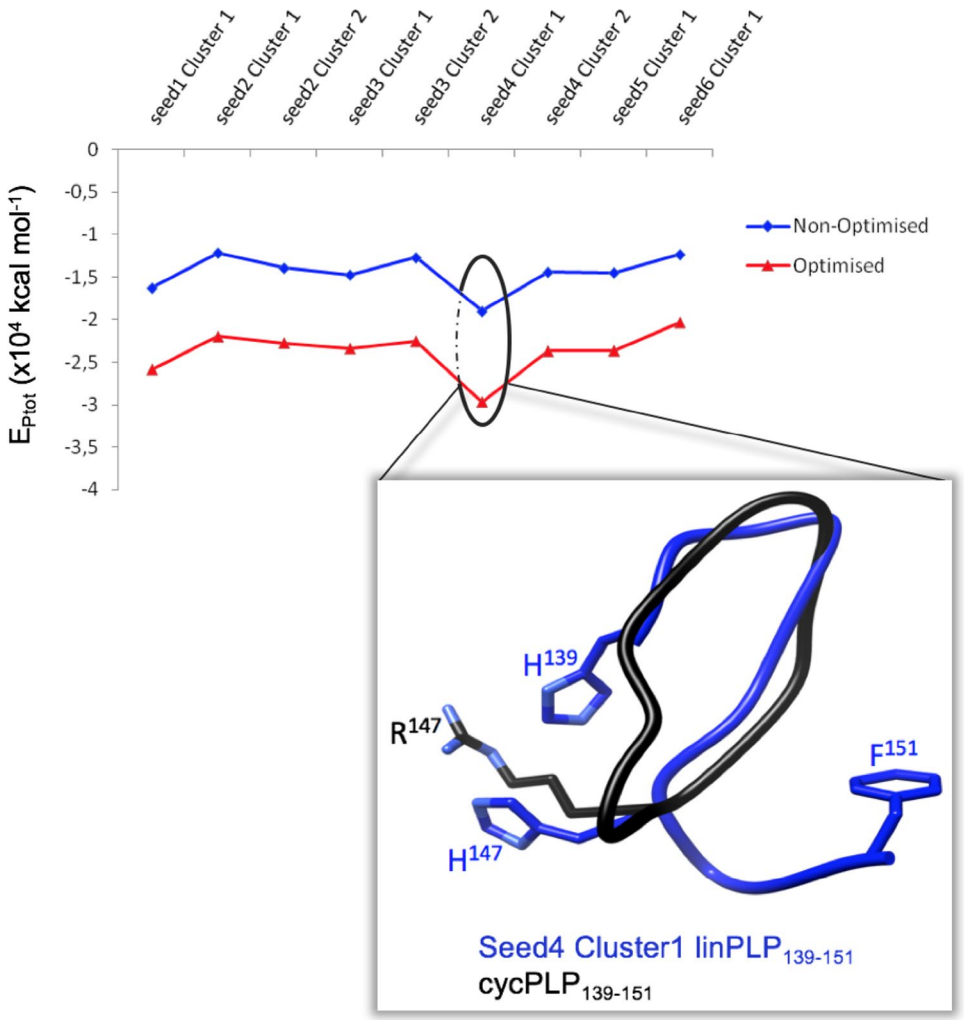

Fig. 7 Graph of potential energy (E_{Ptot}) of the representative conformations before and after geometry optimization. The inserted picture presents the superimposition of $PLP_{139–151}$ cluster with the lowest E_{Ptot} (seed 4, *blue*), with the respective cyclic (139–151) (L^{144}, R^{147}) $PLP_{139–151}$ analogue (*black*)

cyclic (139–151) (L^{144}, R^{147}) $PLP_{139–151}$ analogue (Fig. 7, blue and black).

In order to compare the results produced by the MD simulation and the recorded ROE data of linear $PLP_{139–151}$ peptide, we have looked at the distances between the hydrogen atoms that are connected with the $–C^{\alpha}$ and –N backbone atoms (Fig. S1) in the dominant "sigmoidal" conformation. The majority of these distances, in the MD simulation, are ranging between 2.30 and 2.95 Å (average value). The results are in close agreement with the values reported by the ROE signals (Table 2); variation in the data recorded during the MD run and the NMR, can be attributed to the fact that the ROE values represent averages. Furthermore, the analysis of the distances between protons $H^{N}_{(i)}–H^{\alpha}_{(i+2)}$, $H^{N}_{(i)}–H^{\beta 1}_{(i+2)}$, $H^{N}_{(i)}–H^{\beta 2}_{(i+2)}$ and $H^{N}_{(i)}–H^{R}_{(i+2)}$ for residues Leu^{145}–His^{147}(Fig. 8a, "sigmoidal" form) showed that the distances are comparable to the experimental ROE results reported in Table 2. The comparison between the calculated and the experimental results, suggests the appearance of a fold in this segment of the peptide. Subsequently, the calculated distance (2.0 Å) between the H_N atoms of Leu^{145} and Gly^{146}further supports the above observation.

Respectively, the analysis of the distances in the representative structure of cyclic (139–151) (L^{144}, R^{147}) $PLP_{139–151}$ analogue reveals that the $H^{N}_{(i)}–H^{N}_{(i+1)}$ distances, reported in Table 3, are retained in our simulations studies (Fig. 8b). In addition to the distances between the backbone hydrogens, the long range $H^{\gamma}_{(i)}–H^{N}_{(i+3)}$ distance between Leu^{141} and Leu^{144} is reported to be 5.4 Å in the MD simulation (Fig. 8c) while the $H^{\beta}_{(i)}–H^{N}_{(i+2)}$ reported between Asp^{149} and Phe^{151} is 5.1 Å in the representative conformation (Fig. 8c). These calculated distances are in close agreement with the reported NOE data (Table 3).

Finally, the analysis of the hydrogen bond (HB) interactions in both peptide analogues revealed that there are no substantial HBs formed during the MD simulation time. This particular observation may readily explain the fluctuations observed in the RMSD values (Fig. 5c) in $PLP_{139–151}$ peptide and subsequently, the potential interchange between the different representative conformations (Fig. 6).

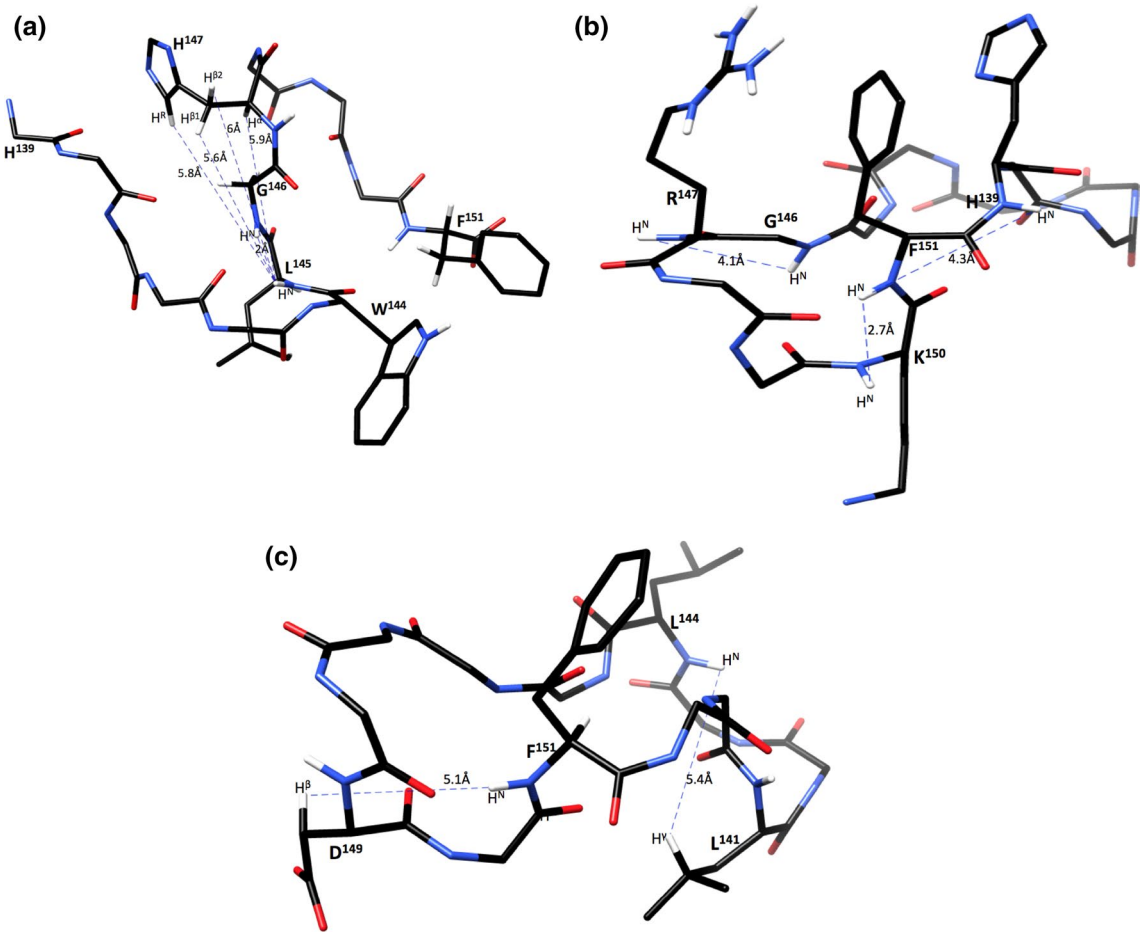

Fig. 8 **a** The representative "sigmoidal" conformation of $PLP_{139–151}$ analogue depicting the $H^{N}_{(i)}–H^{\alpha}_{(i+2)}$, $H^{N}_{(i)}–H^{\beta1}_{(i+2)}$, $H^{N}_{(i)}–H^{\beta2}_{(i+2)}$ and $H^{N}_{(i)}–H^{R}_{(i+2)}$ distances for residues Leu^{145}–His^{147}; Representative conformation of cyclic (139–151) (L^{144}, R^{147}) $PLP_{139–151}$ analogue depicting: **b** the $H^{N}_{(i)}–H^{N}_{(i+1)}$ distances for residues Gly^{146}–Arg^{147}, Lys^{150}–Phe^{151} and Phe^{151}–His^{139}; **c** the long range distances of $H^{\gamma}_{(i)}–H^{N}_{(i+3)}$ between Leu^{141}–Leu^{144} and the $H^{\beta}_{(i)}–H^{N}_{(i+2)}$ between Asp^{149} and Phe^{151}

Conclusions

The analysis of the unrestrained MD simulations of linear $PLP_{139–151}$ peptide revealed the existence of different conformations in aqueous environment (Fig. 6). The linear peptide adopts mainly a "sigmoidal" (semi-extended) conformation (Fig. 6a, blue). Furthermore, the presence of a "cyclic" conformation adopted by $PLP_{139–151}$ (Fig. 6b, red) is observed in our simulation studies. The interchange between cyclic and semi-extended conformations for the peptide may be attributed to its small length, with only 13 amino acids. However, the ROE data, which are in close agreement with the calculated semi-extended conformation, also indicate that this is a dominant conformation of linear peptide in the aqueous environment. The cyclic (139–151) (L^{144}, R^{147}) $PLP_{139–151}$ analogue presents a stable conformation during unrestrained MD simulations with the distances in close agreement with the reported NOE data. The "cyclic" conformation adopted by $PLP_{139–151}$ analogue presents similar structural features with cyclic (139–151) (L^{144}, R^{147}) $PLP_{139–151}$ analogue; the differences between the two peptides are mainly centred, on positions 144 and 147.

The substitutions of Trp^{144} and His^{147} with Leu and Arg, respectively, in the cyclic analogue lead to changes in the orientations of their side chains with respect to the linear analogue either in its semi-extended or "cyclic" form (Figs. 6b, 7), which is the most important feature of the reported conformational analysis. Namely, the change in the orientation, especially for Arg^{147}, could potentially reduce the binding properties of the cyclic analogue with the TCR and could lead to decreased EAE induction. The potential decreased affinity for TCR of the synthesized cyclic analogue, might suggest a similar mode of action with other synthesized cyclic peptide analogues of myelin proteins reported in our previous studies [15–17, 23, 26]. Further studies, regarding the impact of mutations in the PLP epitope (linear and cyclic), could be carried

out to expand our understanding of the trimolecular complex formation (TCR-peptide-MHC or HLA) and T cell stimulation.

Acknowledgements This work was supported by the "Cooperation Program" [Grant No. 09SYN21-609] and by "Cooperation Greece-Israel Program" [Grant No. ISR-3148] O.P. Competitiveness & Entrepreneurship (EPAN II), ROP Macedonia- Thrace, ROP Crete and Aegean Islands, ROP Thessaly- Mainland Greece- Epirus, ROP Attica and Slovenian Research Agency [Grant No. P1-0010]. We also thank FICYT and the European Union (7th WP) for a Marie Curie CLARIN-cofund fellowship to CS. The authors acknowledge the contribution of Agathi Nteli in synthesis of PLP peptide analogues.

Compliance with ethical standards

Conflict of interest The authors declare that they have no conflict of interest.

References

1. Steinman L (1996) Multiple sclerosis: a coordinated immunological attack against myelin in the central nervous system. Cell 85:299–302
2. Noseworthy JH, Lucchinetti C, Rodriguez M, Weinshenker BG (2000) Multiple sclerosis. N Engl J Med 343:938–952
3. Shahrizaila N, Yuki N (2011) Guillain-barré syndrome animal model: the first proof of molecular mimicry in human autoimmune disorder. J Biomed Biotechnol 2011:829129
4. Smith KJ, Pyrdol J, Gauthier L, Wiley DC, Wucherpfennig KW (1998) Crystal structure of HLA-DR2 (DRA*0101, DRB1*1501) complexed with a peptide from human myelin basic protein. J Exp Med 188:1511–1520
5. Jahn O, Tenzer S, Werner HB (2009) Myelin proteomics: molecular anatomy of an insulating sheath. Mol Neurobiol 40:55–72
6. Zamvil SS, Steinman L (1990) The T lymphocyte in experimental allergic encephalomyelitis. Annu Rev Immunol 8:579–621
7. Pelfrey CM, Tranquill LR, Vogt AB, McFarland HF (1996) T cell response to two immunodominant proteolipid protein (PLP) peptides in multiple sclerosis patients and healthy controls. Mult Scler 1:270–278
8. Steinman L (1999) Assessment of animal models for MS and demyelinating disease in the design of rational therapy. Neuron 24:511–514
9. Anderson AC, Nicholson LB, Legge KL, Turchin V, Zaghouani H, Kuchroo VK (2000) High frequency of autoreactive myelin proteolipid protein–specific T cells in the periphery of naive mice. J Exp Med 191:761–770
10. Katsara M, Tselios T, Deraos S, Deraos G, Matsoukas M-T, Lazoura E, Matsoukas J, Apostolopoulos V (2006) Round and round we go: cyclic peptides in disease. Curr Med Chem 13:2221–2232
11. Tuohy VK, Lu Z, Sobel RA, Laursen RA, Lees MB (1989) Identification of an encephalitogenic determinant of myelin proteolipid protein for SJL mice. J Immunol 142:1523–1157
12. Greer JM, Kuchroo VK, Sobel R a, Lees MB (1992) Identification and characterization of a second encephalitogenic determinant of myelin proteolipid protein (residues 178–191) for SJL mice. J Immunol 149:783–788
13. Greer JM, Sobel RA, Sette A, Southwood S, Lees MB, Kuchroo VK (1996) Immunogenic and encephalitogenic epitope clusters of myelin proteolipid protein. J Immunol 156:371–379
14. Kuchroo VK, Greer JM, Kaul D, Ishioka G, Franco A, Sette A, Sobel RA, Lees MB (1994) A single TCR antagonist peptide inhibits experimental allergic encephalomyelitis mediated by a diverse T cell repertoire. J Immunol 153:3326–3336
15. Matsoukas J, Apostolopoulos V, Kalbacher H, Papini A-M, Tselios T, Chatzantoni K, Biagioli T, Lolli F, Deraos S, Papathanassopoulos P, Troganis A, Mantzourani E, Mavromoustakos T, Mouzaki A (2005) Design and synthesis of a novel potent myelin basic protein epitope 87–99 cyclic analogue: enhanced stability and biological properties of mimics render them a potentially new class of immunomodulators. J Med Chem 48:1470–1480
16. Potamitis C, Matsoukas M-T, Tselios T, Mavromoustakos T, Golič Grdadolnik S (2011) Conformational analysis of the MBP83–99 (Phe91) and MBP83–99 (Tyr91) peptide analogues and study of their interactions with the HLA-DR2 and human TCR receptors by using molecular dynamics. J Comput Aided Mol Des 25:837–853
17. Tselios T, Aggelidakis M, Tapeinou A, Tseveleki V, Kanistras I, Gatos D, Matsoukas J (2014) Rational design and synthesis of altered peptide ligands based on human myelin oligodendrocyte glycoprotein 35–55 epitope: inhibition of chronic experimental autoimmune encephalomyelitis in mice. Molecules 19:17968–17984
18. Katsara M, Deraos S, Tselios T V, Pietersz G, Matsoukas J, Apostolopoulos V (2014) Immune responses of linear and cyclic PLP 139–151 mutant peptides in SJL/J mice: peptides in their free state versus mannan conjugation. Immunotherapy 6:709–724
19. Tapeinou A, Matsoukas M-T, Simal C, Tselios T (2015) Cyclic peptides on a merry-go-round; towards drug design. Biopolymers 104:453–461
20. Namjoshi S, Benson HAE (2010) Cyclic peptides as potential therapeutic agents for skin disorders. Biopolymers 94:673–680
21. Li X, Peterkofsky A, Wang G (2008) Solution structure of NPr, a bacterial signal-transducing protein that controls the phosphorylation state of the potassium transporter-regulating protein IIANtr. Amino Acids 35:531–539
22. Pellecchia M, Bertini I, Cowburn D, Dalvit C, Giralt E, Jahnke W, James TL, Homans SW, Kessler H, Luchinat C, Meyer B, Oschkinat H, Peng J, Schwalbe H, Siegal G (2008) Perspectives on NMR in drug discovery: a technique comes of age. Nat Rev Drug Discov 7:738–745
23. Mantzourani ED, Tselios TV, Grdadolnik SG, Platts JA, Brancale A, Deraos GN, Matsoukas JM, Mavromoustakos TM (2006) Comparison of proposed putative active conformations of myelin basic protein epitope 87–99 linear altered peptide ligands by spectroscopic and modelling studies: the role of positions 91 and 96 in T-cell receptor activation. J Med Chem 49:6683–6691
24. Mantzourani ED, Platts JA, Brancale A, Mavromoustakos TM, Tselios TV (2007) Molecular dynamics at the receptor level of immunodominant myelin basic protein epitope 87–99 implicated in multiple sclerosis and its antagonists altered peptide ligands: triggering of immune response. J Mol Graph Model 26:471–481
25. Mantzourani ED, Blokar K, Tselios TV, Matsoukas JM, Platts JA, Mavromoustakos TM, Grdadolnik SG (2008) A combined NMR and molecular dynamics simulation study to determine the conformational properties of agonists and antagonists against experimental autoimmune encephalomyelitis. Bioorg Med Chem 16:2171–2182
26. Yannakakis MP, Tzoupis H, Michailidou E, Mantzourani E, Simal C, Tselios T (2016) Molecular dynamics at the receptor level of immunodominant myelin oligodendrocyte glycoprotein 35–55 epitope implicated in multiple sclerosis. J Mol Graph Model 68:78–86

27. Barlos K, Chatzi O, Gatos D, Stavropoulos G (1991) 2-Chlorotrityl chloride resin: studies on anchoring of Fmoc-amino acids and peptide cleavage. Int J Pept Protein Res 37:513–520
28. Tselios T, Probert L, Daliani I, Matsoukas E, Troganis A, Gerothanassis IP, Mavromoustakos T, Moore GJ, Matsoukas JM (1999) Design and synthesis of a potent cyclic analogue of the myelin basic protein epitope MBP 72–85: importance of the Ala 81 carboxyl group and of a cyclic conformation for induction of experimental allergic encephalomyelitis. J Med Chem 42:1170–1177
29. Tselios T, Daliani I, Deraos S, Thymianou S, Matsoukas E, Troganis A, Gerothanassis I, Mouzaki A, Mavromoustakos T, Probert L, Matsoukas J (2000) Treatment of experimental allergic encephalomyelitis (EAE) by a rationally designed cyclic analogue of myelin basic protein (MBP) epitope 72–85. Bioorg Med Chem Lett 10:2713–2717
30. Ieronymaki M, Androutsou ME, Pantelia A, Friligou I, Crisp M, High K, Penkman K, Gatos D, Tselios T (2015) Use of the 2-chlorotrityl chloride resin for microwave-assisted solid phase peptide synthesis. Biopolymers 104:506–514
31. Tselios T, Apostolopoulos V, Daliani I, Deraos S, Grdadolnik S, Mavromoustakos T, Melachrinou M, Thymianou S, Probert L, Mouzaki A, Matsoukas J (2002) Antagonistic effects of human cyclic MBP 87–99 altered peptide ligands in experimental allergic encephalomyelitis and human T-cell proliferation. J Med Chem 45:275–283
32. Pettersen EF, Goddard TD, Huang CC, Couch GS, Greenblatt DM, Meng EC, Ferrin TE (2004) UCSF chimera—a visualization system for exploratory research and analysis. J Comput Chem 25:1605–1612
33. Case DA, Berryman JT, Betz RM, Cerutti DS, Cheatham, III TE, Darden TA, Duke RE, Giese TJ, Gohlke H, Goetz AW, Homeyer N, Izadi S, Janowski P, Kaus J, Kovalenko A, Lee TS, LeGrand S, Li P, Luchko T, Luo R, Madej B, Merz KM, Monard P, Needham HT, Nguyen H, Omelyan I, Onufriev A, Roe DR, Roitberg A, Salomon-Ferrer R, Simmerling CL, Smith W, Swails J, Walker RC, Wang J, Wolf RM, Wu X, York DM, Kollman P (2015) AMBER 2015. University of California, San Francisco
34. Maier JA, Martinez C, Kasavajhala K, Wickstrom L, Hauser KE, Simmerling C (2015) ff14SB: improving the accuracy of protein side chain and backbone parameters from ff99SB. J Chem Theory Comput 11:3696–3713
35. Jorgensen WL, Chandrasekhar J, Madura JD, Impey RW, Klein ML (1983) Comparison of simple potential functions for simulating liquid water. J Chem Phys 79:926–935
36. Izaguirre JA, Catarello DP, Wozniak JM, Skeel RD (2001) Langevin stabilization of molecular dynamics. J Chem Phys 114:2090–2098
37. Ryckaert J-P, Ciccotti G, Berendsen HJC (1977) Numerical integration of the cartesian equations of motion of a system with constraints: molecular dynamics of n-alkanes. J Comput Phys 23:327–341
38. Darden T, York D, Pedersen L (1993) Particle mesh Ewald: an N ·log(N) method for Ewald sums in large systems. J Chem Phys 98:10089–10092
39. Roe DR, Cheatham TE (2013) PTRAJ and CPPTRAJ: software for processing and analysis of molecular dynamics trajectory data. J Chem Theory Comput 9:3084–3095
40. Shao J, Tanner SW, Thompson N, Cheatham TE (2007) Clustering molecular dynamics trajectories: 1. characterizing the performance of different clustering algorithms. J Chem Theory Comput 3:2312–2334
41. Spyranti Z, Dalkas GA, Spyroulias GA, Mantzourani ED, Mavromoustakos T, Friligou I, Matsoukas JM, Tselios TV (2007) Putative bioactive conformations of amide linked cyclic myelin basic protein peptide analogues associated with experimental autoimmune encephalomyelitis. J Med Chem 50:6039–6047